Combustion and Flame 215 (2020) 324–332

Contents lists available at ScienceDirect

Combustion and Flame

journal homepage: www.elsevier.com/locate/combustflame

Synthesis, characterization and nanoenergetic utilizations of fluorine, oxygen co-functionalized graphene by one-step XeF_2 exposure

Anqi Wang[a], Sangho Bok[b,c], Cherian Joseph Mathai[c], Rajagopalan Thiruvengadathan[c], Charles M. Darr[c], H. Chen[e], Michael R. Zachariah[f], Keshab Gangopadhyay[c], Jacob A. McFarland[d], Matthew R. Maschmann[c,d,*], Shubhra Gangopadhyay[c,**]

[a] Department of Biomedical, Biological, and Chemical Engineering, University of Missouri, Columbia, MO 65211, United States
[b] Department of Engineering and Technology, Southern Utah University, Cedar City, UT 84720, United States
[c] Department of Electrical Engineering and Computer Science, University of Missouri, Columbia, MO 65211, United States
[d] Department of Mechanical and Aerospace Engineering, University of Missouri, Columbia, MO 65211, United States
[e] Department of Chemical Engineering, University of Maryland, College Park, MD 20740, United States
[f] Department of Chemical Engineering and Material Science, University of California, Riverside, CA 95207, United States

ARTICLE INFO

Article history:
Received 8 August 2019
Revised 2 February 2020
Accepted 6 February 2020

Keywords:
Nanomaterial
Graphene
Fluorinated graphene
Nanothermite

ABSTRACT

The energetic performance of aluminum(Al)-based nanothermite composites is hindered by the native alumina shell on the surface of Al nanoparticles. To maximize the energetic release and lower the reaction temperature between Al and metal oxide nanoparticles, a novel fluorine and oxygen co-functionalized graphene (FGO) is reported. The material was synthesized by gas–solid reaction between graphene oxide paper and XeF_2 gas. The stability of FGO in atmospheric humidity, heating, and exfoliation by sonication in different solvents were obtained by FTIR and SEM-EDS. The FGO contained both unstable acyl fluoride groups and stable carbon-fluorine covalent/semi-ionic bonds in its structure. The FGO was introduced as a functional additive in an Al/Bi_2O_3 nanothermite composite, leading to a heat of reaction heat of 1123 J/g, 58% greater than that from loose Al/Bi_2O_3 powder. The reaction completed before reaching the melting temperature of Al, indicating a novel all-solid-state reaction between Al and Bi_2O_3. The decreased reaction temperature is attributed to fluorine etching of the native alumina shell surrounding the Al nanoparticle fuel.

1. Introduction

Following the fluorination of bulk graphite in 1934 [1], exploration of fluorinated carbon-based materials has steadily increased [2,3]. Fluorographite [4,5], which is commonly used as a lubricant [6], biomolecular sensing agent [7], and cathode in lithium cell [8], is prepared by bonding fluorine to sp^2 carbon materials. Fluorine-functionalized polymers, consisting of fluorine atoms bonded to a carbon skeleton, form the basis commonly-used materials such as polytetrafluoroethylene (PTFE) [9-11]. More recently, fluorination of carbon nanomaterials such as C_{60} [12], carbon nanotubes [13,14] and graphene [15,16] has been demonstrated. Graphene has been widely researched to exploit its high thermal and electrical conductivity, mechanical strength, and unique optical properties [17,18]. These properties are altered after fluorination due to the strong electronegativity of fluorine. As a result, fluorinated graphene has been applied in high-performance supercapacitors [19], anode material for lithium-ion batteries [20], optical limiting devices [21], and transistors [22].

Various methods have been developed to obtain fluorinated graphene with different F/C ratios [23]. Gas–solid reactions between F_2 and graphene oxide (GO) [24], or between XeF_2 and chemical vapor deposition (CVD) graphene [15,25] generated fluorinated graphene with an F/C ratio approaching unity. Plasma fluorination of graphene and GO using inorganic fluorine compounds such as SF_6 [26], CF_4 [27] or argon/F_2 [28], provided a mild F/C ratio up to 0.3. Other chemical methods such as hydrothermal (F/C up to 0.48) [29,30] and photochemical fluorination (F/C up to 0.33) [31], or physical exfoliation of fluorographite (F/C up to 1.00) [32,33] were also employed to obtain fluorinated graphene. Of these techniques, gaseous fluorination provided the highest capacity and controllability for fluorine loading; however, the toxic-

* Corresponding author at: Department of Mechanical and Aerospace Engineering, Univeristy of Missouri, Columbia, MO 65211, United States.
** Corresponding author at: Department of Electrical Engineering and Computer Science, University of Missouri, Columbia, MO 65211, United States.
E-mail addresses: maschmannm@missouri.edu (M.R. Maschmann), gangopadhyays@missouri.edu (S. Gangopadhyay).

https://doi.org/10.1016/j.combustflame.2020.02.005
0010-2180/

Nomenclature

GO	graphene oxide
FGO	fluorinated graphene oxide
XeF_2	xenon difluoride
$NaNO_3$	sodium nitrate
$KMnO_4$	potassium permanganate
H_2O_2	hydrogen peroxide
IPA	isopropanol/isopropyl alcohol
THF	tetrahydrofuran
PC	propylene carbonate
PTFE	polytetrafluoroethylene
THV	terpolymer of tetrafluoroethylene, hexafluoropropylene and vinylidene fluoride
CVD	chemical vapor deposition
FTIR	Fourier-transform infrared spectroscopy
DSC	differential scanning calorimetry
TGA	THERMOGRAVIMETRIC analysis
XRD	x-ray powder diffraction

ity of F_2 gas limits its wide application [24]. Previous investigation of XeF_2 has been limited to CVD graphene, leading to fluorinated graphene without oxygen functional groups, limiting its further applications [25]. Fluorinating GO using XeF_2 has not previously been previously reported and may facilitate partial retention of oxygen functional groups and enable the production of chemically functionalized fluorinated graphene oxide (FGO).

While graphene and GO scaffolds have been recently been utilized to increase the energy release and reaction rate in nanothermite materials [34–37], fluorinated graphene has not previously been examined in this way. A typical nanothermite material is a binary mixture composed of a solid-state fuel (Al, Mg, Si, B, etc.) and a nanoparticle oxidizer (normally metal oxide). Al-based nanothermites are widely investigated because of the abundance of Al, and its large mass-specific energy release [38]. The native alumina shell on the surface of Al nanoparticles, however, severely restricts access to the Al core and reduces the reaction rate of the material. The role of the rigid shell in the reaction mechanism is not fully understood, complicating the optimization of Al-based nanothermite composites [39–41]. Fluorine species may exothermally react with and etch the alumina shell in a nanothermite composite, allowing both access of the Al core to external species and the diffusion of Al from the shell. The al fuel may then react with oxidizer, even below the Al melting temperature. These so-called preignition reactions between the alumina shell and fluorine species have been observed during the decomposition of fluoropolymers such as PTFE and THV [42,43]. Delivery of fluorine species to Al fuel particles by other constituent materials, such as fluorinated graphene or GO, has not been explored.

Here we report a parametric study of GO fluorination using XeF_2, with a targeted application in nanothermite composites. The FGO samples contained both fluorine functional groups and oxygen functional groups, enabling further functionalization and modification of the material with additional processing. Using FTIR and XRD, functionalized samples were found to undergo changes of functional groups such as the hydrolysis of acyl fluoride groups in air. The release of fluorine from the material with heating was confirmed by mass spectrometry, TGA, and EDS. The FGO material was then utilized as an additive for both Al nanoparticles and Al/Bi_2O_3 nanothermite composites. DSC results indicate the FGO enhanced the energetic performance and decreased the reaction temperature for Al-based nanothermites.

2. Experimental details

GO paper was produced by the modified Hummer's method [34]. In brief, 1 g graphite (×GnP science, 5 μm) and 1 g $NaNO_3$ (Aldrich) were dispersed in concentrated 46 mL H_2SO_4 (Fluka) cooled by ice/water bath under magnetic stirring. Next, 6 g of $KMnO_4$ (Aldrich) was gradually added to the mixture while keeping the dispersion under 20 °C. Subsequently, the mixture was heated to 35 °C for a duration of 1 h. 80 mL of water was added, and the mixture was heated to 80 °C for 30 min. After cooling, 6 mL H_2O_2 (Fluka) was added to the mixture to terminate the reaction. The GO product was then purified by repeatedly washing with water and centrifugation until the resultant supernatant turns neutral. Finally, the dispersion was sonicated in water at a concentration of approximately 3 mg/mL and dried at 70 °C overnight to obtain GO paper.

A custom-built pulsed xenon difluoride (XeF_2) reaction system was used for the fluorination of GO paper. XeF_2 in its vapor phase is pulsed into the reacting chamber until the pressure in the chamber reached 3000 mTorr, and the reaction of GO paper with XeF_2 was carried out for 10 min before the reaction chamber was purged with N_2 to complete one cycle of the pulsed reaction. Two sets of fluorinated GO paper were synthesized under room temperature, one with 130 pulsed cycles corresponding to 1300 min of XeF_2 treatment, labeled as FGO-I, and the other with 270 cycles corresponding to 2700 min of XeF_2 treatment, labeled as FGO-II. After reaction, the samples were stored in a desiccator at approximately 15% humidity and 25 °C before further characterization.

GO/Al and FGO/Al samples were prepared using the following procedure. FGO samples were used immediately after XeF_2 treatment. GO and FGO were first dispersed in isopropanol (IPA, anhydrous grade, Fluka) at a concentration of 2 mg/mL by sonication for 5 h. Separately, Al nanoparticles (Novacentrix, 80 nm average diameter with 2.2 nm Al_2O_3 shell, 79% reactive) were dispersed in IPA at a concentration of 20 mg/mL for 4 h. The Al dispersion was then added to the FGO or GO dispersion in pre-determined quantities, and sonication for an additional 4 h. The mixture was then dried under vacuum.

Al/Bi_2O_3 nanothermite (Al/Bi_2O_3 equivalence ratio = 1.4) was synthesized by 5-hour sonication. Bi_2O_3 nanoparticles (Aldrich, 200 nm) were first sonicated in IPA (400 mg in 1.2 mL) for 1 h. Thereafter, 82 mg of Al nanoparticles were added directly to the Bi_2O_3/IPA dispersion and sonicated for an additional 4 h. The dispersion was then dried under vacuum [34].

The $FGO/Al/Bi_2O_3$ and $GO/Al/Bi_2O_3$ nanothermite composite were prepared by a similar 9-h sonication process. FGO was dispersed in IPA at a concentration of 2 mg/mL by sonication for 5 h. Simultaneously, Al /Bi_2O_3 was prepared in IPA using the 5-h sonication process described above. The Al/Bi_2O_3 dispersion was then added to the FGO dispersions and sonicated for an additional 4 h. The mixture was then dried under vacuum. FGO and GO occupied 5% of total mass in the nanothermite composite, and the equivalence ratio between Al and Bi_2O_3 was 1.4 (fuel rich). A control Al/Bi_2O_3 sample was also prepared separately to compare the energy release with the $FGO/Al/Bi_2O_3$ and $GO/Al/Bi_2O_3$ sample.

Thermogravimetry and differential scanning calorimetry (DSC-TGA) was carried out (TA Instruments SDT-Q600) at a heating rate of 20 °C min^{-1} under argon flow at 200 mL min^{-1}. Samples were placed in Pt crucibles during heating.

Fourier-transform infrared spectroscopy (FTIR) spectrum was measured by a Thermo Nicolet Nexus 4700 FTIR spectrometer. Attenuated total reflectance (ATR) was carried out on a germanium stage.

Mass spectrometry was carried out by a T-jump [44] mass spectrometry hybrid system. The FGO sample was dispersed in IPA and coated on a Pt filament. The Pt filament was heated at a rate of

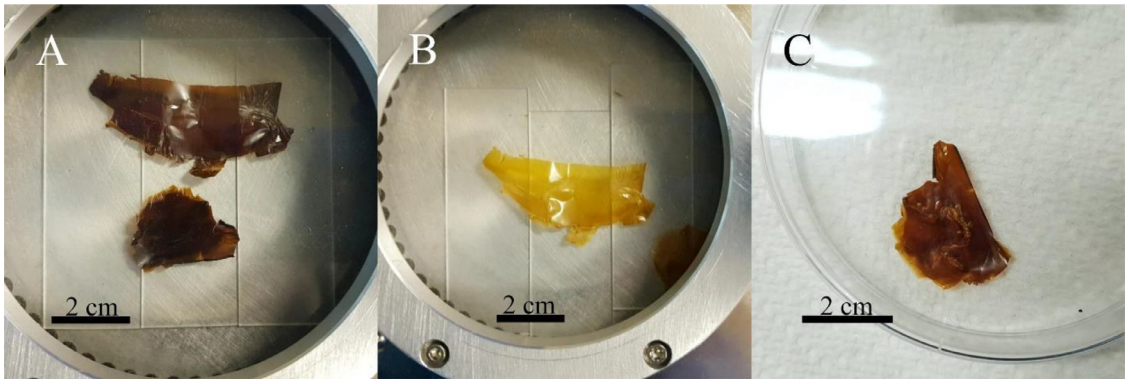

Fig. 1. Optical pictures of GO (A) FGO-I right after XeF_2 treatment (B) and after 3 days in desiccator (15% humidity) (C).

~3 × 10^5 K/s, producing decomposition products which were ionized at 70 eV and analyzed by a time-of-flight mass spectrometer.

X-ray diffraction (XRD) patterns were recorded on a Rigaku Ultima IV powder X-ray diffractometer operated at 44 kV and 44 mA using a copper X-ray radiation (λ = 1.5438 Å). Samples were scanned from 5° to 60° (2θ) with a step size of 0.02° and at a scanning speed of 2°/min.

X-ray Energy Dispersive Spectroscopy (EDS) was analyzed by using Bruker Quantax 200 Silicon Drift Detector with Xflash6 with a FEI Quanta 600 FEG Environmental Scanning Electron Microscope. Measurements were taken at low vacuum mode at 50 Pa water vapor to compensate the low conductivity of the material.

3. Results and discussion

GO paper underwent a color change as a result of the XeF_2 fluorination process, as shown in Fig. 1. The initial GO paper was dark brown (Fig. 1(A)). After 1300 min of XeF_2 treatment, the FGO paper was a light, translucent yellow (Fig. 1(B)), similar to fluorination of GO by F_2 [24]. After three days in a desiccator chamber, the FGO paper turned light brown, indicating further composition change (Fig. 1(C)). The FGO-II sample (2700 min exposure) showed a similar color change.

FTIR measurements showed distinct changes in the chemical structure of GO after reaction with XeF_2, as shown in Fig. 2(A). The strong peak present in GO located at 3000–3700 cm^{-1}, corresponds to the O–H stretching in C–OH groups and –COOH groups, was significantly reduced in FGO-I after reaction with XeF_2 for 1300 min, and almost disappeared in FGO-II after 2700 min, indicating the replacement of hydroxyl groups by fluoride groups. Previous reports showed that the bonded hydrogen atoms in macromolecules, such as polymers, could be readily substituted by fluorine [45], and the potential HF product might further catalyze the fluorination reaction [46]. The absorption band at 1730 cm^{-1}, attributed to the C=O stretching in the GO structure, remained similar after XeF_2 treatment, indicating no significant reaction between the carbonyl groups in GO and XeF_2. The asymmetric and symmetric stretching of –COO– in the carboxyl acid groups in GO, shown by the absorption bands at 1620 cm^{-1} and 1420 cm^{-1}, respectively, were reduced significantly after reaction. Correspondingly, an extra absorption band appeared at 1840 cm^{-1}, representing the C=O stretching in acyl fluoride (F–C=O), produced by the substitution of –OH groups in carboxyl acid by fluorine atoms. The absorption bands for stretching of the C–O bond in C–O–C and C–OH groups at 1220 cm^{-1} and 1050 - 1060 cm^{-1} were also diminished. The sharp peak at 1235 cm^{-1} reflects the formation of C-F covalent bonding, the chemical bond between fluorine and sp^3 hybridized carbon. The peak near 1140 cm^{-1} in FGO-I revealed the formation of the semi-ionic C–F bond between fluorine and sp^2 hybridized carbon, which was also found in the carbon fluorinated nanotube produced below 100 °C [23,47]. In FGO-II, the peak shifted to around 1100 cm^{-1}, indicating the formation of CF_x (x>1) in the structure. The presence of these unique peaks indicated the successful fluorination of GO after fluorination reaction by using XeF_2 gas for 1300 or 2700 min. A scheme of the reaction is included in Fig. 2(B).

The XRD results of GO and FGO-I are shown in supporting information (Fig. S1 and Table S1). The XRD spectra of GO and FGO-I was measured in the range of 5°–60° and both the samples shows a peak (001) at 2θ ~ 10.5°. Due to fluorination of GO, there is small change in the peak (001) value. It is postulated that oxygen-containing groups in the stacking were replaced by fluorine atoms, thereby changing the interlayer distance (d) shown in the Table S1. It is also noted that the FWHM of FGO increased, an indication of a lower degree of crystallinity as compared to GO. Due to a small change in the interlayer distance (d), the majority of oxygen func-

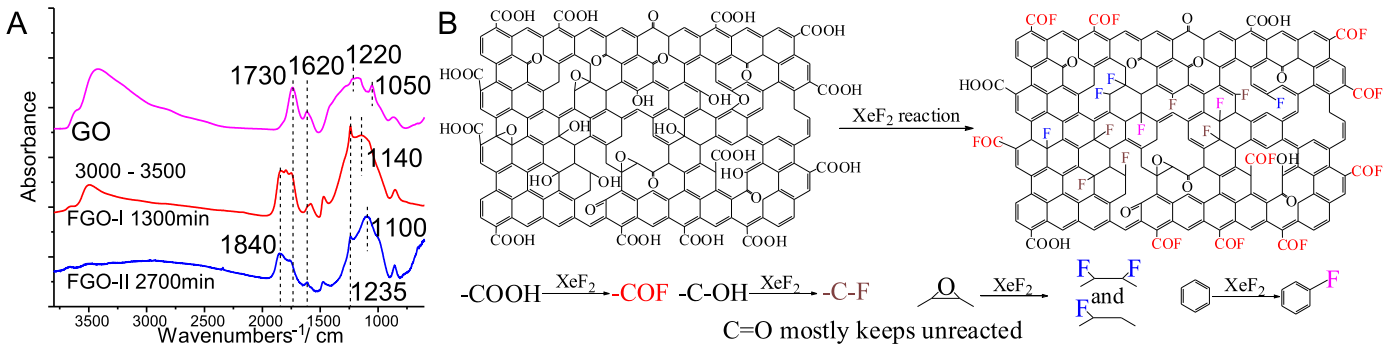

Fig. 2. FTIR curves of GO, FGO-I (1300 min) and FGO-II (2700 min) (A) and scheme of reactions during the XeF_2 treatment (B).

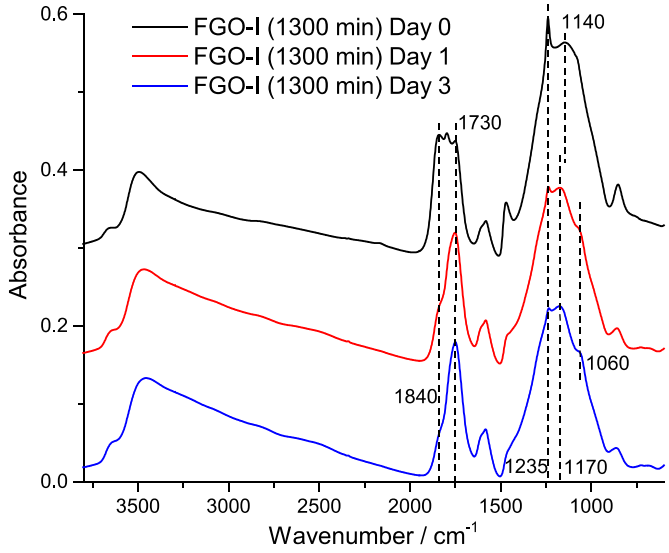

Fig. 3. FTIR curves of GO and FGO-I (Reacted with XeF_2 for 1300 min) after storage in a desiccator.

tional groups remained in the structure, suggesting only minor incorporation of fluorine atoms during the XeF_2 treatment of GO.

FTIR was also employed to investigate the stability in the FGO structure with time when stored in a desiccator environment (~15% humidity), as shown in Fig. 3. After 3 days stored in the desiccator, the absorption band of C=O stretching in acyl fluoride (1840 cm^{-1}) was significantly reduced, remaining only as a small shoulder due to the hydrolysis reaction of acyl fluoride groups with free water in atmosphere (-COF + H_2O → -COOH + HF). The –OH absorption band from 3200 to 3700 cm^{-1} slightly increased due to the same process. Additionally, the sharp C–F covalent peak at 1235 cm^{-1} was reduced, and the C–F semi-ionic peak around 1140 cm^{-1} also shifted to around 1170 cm^{-1}, indicating the decomposition of some C–F bonds in the structure. This result corresponds with the results reported by Stine et al. that fluorine bonded with the basal plane of carbon decomposed with storage time [25]. A small shoulder also appeared at 1060 cm^{-1}, indicating the formation of more C–OH groups during storage. Therefore, after GO was fluorinated by XeF_2, reactions with residual atmospheric water vapor lead to a gradual loss of the fluorine functional groups and a return back to a structure similar to GO. The scheme of the material change during storage is included in Figure S2.

DSC-TGA was also carried out to measure the thermal stability of FGO samples with time. Results are shown in Fig. 4. Neat GO paper was examined as a baseline. The GO paper decomposed exothermically from 150 °C to 300 °C, with a peak energy release at 178 °C. Newly prepared FGO-I samples began losing mass at 245 °C, while samples stored in a desiccator for 2 weeks began losing mass at 219 °C, as shown in Fig. 4(B). The mass loss of GO and exothermal reactions were attributed to the decomposition process of oxygen-containing functional groups, including hydroxyl, epoxide, carbonyl and carboxyl groups. Fig. 4(B) shows that the mass loss can be divided into two different stages. Stage I is from 150 °C to around 210 °C, represented by a peak in the differential thermal gravimetry (DTG) curve in Fig. 4B, indicating the evaporation of trapped water and removal of labile oxygen functional groups such as epoxyl or hydroxyl groups in the basal plane of graphene [48,49]. Stage II occurred from 210 °C to about 300 °C and reflected a slower mass loss. The removal of more stable oxygen functional groups, such as carboxyl and carbonyl groups, occurred in this stage. In the DTG curve of the FGO-I sample shortly after fluorination in Fig. 4(B) (Day 1), the initiation of mass loss occurred

Table 1
Composition of FGO-I after heating to different temperatures by SEM-EDS.

Temperature	Element content (atomic)			Element ratio	
	Carbon (%)	Oxygen (%)	Fluorine (%)	C/O	F/O
No heating	51.5	36.9	11.0	1.43	0.306
150 °C	54.8	37.6	6.8	1.43	0.180
300 °C	68.5	27.6	2.4	2.48	0.085
450 °C	77.2	20.6	0.6	3.74	0.027
600 °C	83.4	14.7	0.4	5.66	0.028

at 210 °C, indicating that most labile epoxyl and hydroxyl groups had been removed from the structure during XeF_2 treatment. After 16 days of storage, the decomposition temperature of FGO-I reduced to 219 °C, indicating that some of the fluorinated groups decomposed during storage. Meanwhile, the temperature associated with peak energy release also decreased in FGO-I sample with storage time based on DSC results, shown in Fig. 4C. The total energy release also decreased with storage, revealing that some fluorine functional groups were unstable at room temperature. The material reacted spontaneously and reached a state with lower energy. Note that a trend towards decreased decomposition temperature, reaction temperature, and energy loss are observed for intermediate days of desiccator storage. More detailed change in functional groups will be discussed below with FTIR results.

FGO-II showed similar DSC-TGA trends, as observed in Figure S3. The FGO-II sample contained a greater quantity of fluorine and produced a greater decomposition temperature compared to FGO-I at comparable storage times. The integrated energy release during decomposition, the peak temperature of mass loss and the peak temperature of heat release reduced significantly after 2 weeks of storage. It also confirmed that XeF_2-treated GO might return to a structure similar to GO during storage due to the reaction and decomposition of some fluorine functional groups. However, the DSC-TGA data after Day 1 and Day 7 of storage were very similar. This result is in contrast to those of FGO-I which showed a significant difference even after 3 days of storage. Therefore, increased fluorine content seems to have increased the stability of FGO to moisture.

To further investigate FGO decomposition during heating, the elemental composition of FGO-I was measured by SEM-EDS after heating to 150 °C, 300 °C, 450 °C, and 600 °C and held isothermally for 5 min. The results are listed in Table 1. After 1300 min of XeF_2 treatment, the fluorine content was approximately 11 at.%. Upon heating to 150 °C, and before the main decomposition starts (as identified by DSC-TGA), the fluorine content decreased to approximately 7%, implying that some fluorine species were extremely unstable and may be associated as intercalated fluorine molecules, such as HF, stabilized between GO sheets due to the intermolecular forces. Note that while the F/O ratio decreased, the C/O ratio remained stable when heated to 150 °C, indicating the reduction of GO did not commence prior to 150 °C. At higher temperatures, the C/O ratio increased as the oxygen functional groups in FGO reduced. At the same time, the fluorine content decreased at a faster rate than oxygen, as confirmed by the decreasing F/O ratio with temperature.

FTIR-ATR spectra on heated samples are shown in Fig. 5. The change of different functional groups can be clearly seen. Acyl fluoride (F–C=O, shoulder at 1840 cm^{-1}) reduced after heating to 150 °C, and disappeared at 300 °C. The C-F covalent bond (1235 cm^{-1}, as denoted by the short orange line to the left of C–O–C peak in Fig. 5) showed a small peak in unheated samples and those heated to 150 °C but reduced after heating to 300 °C and disappeared at higher temperatures. C–F semi-ionic bond (1140 cm^{-1}) also significantly reduced after heating to 300 °C. After being heated to 600 °C, all other peaks disappeared except

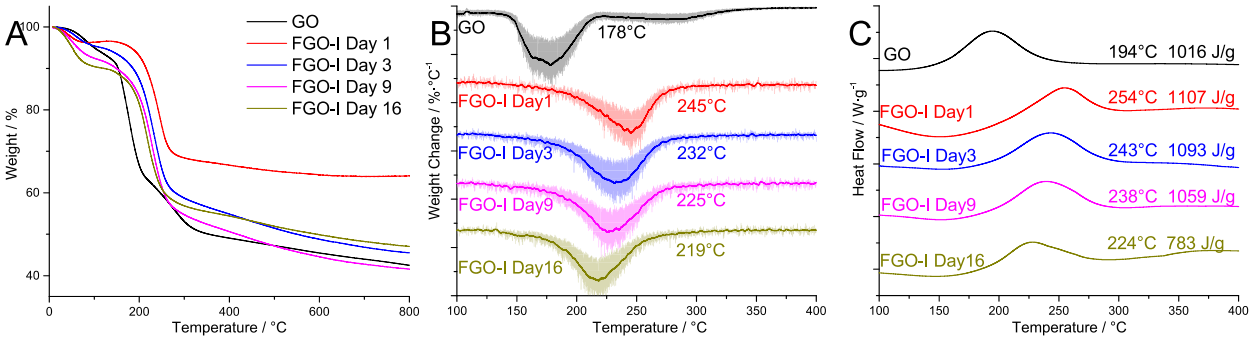

Fig. 4. TGA (A), DTG (B) and DSC(C) curves of FGO-I for a storage duration of up to 16 days after synthesis. In (B), half transparent background is the differential of TGA, while the solid curve represents the smoothed data. The temperature indicates the peak temperature of the smoothed line for each sample. (C) shows DSC curves from GO and FGO samples after various storage times. The temperature shown above the DSC curves represents the peak of DSC curves, and the energy release is obtained from the integration of the heat flow peak. Upward is exothermic.

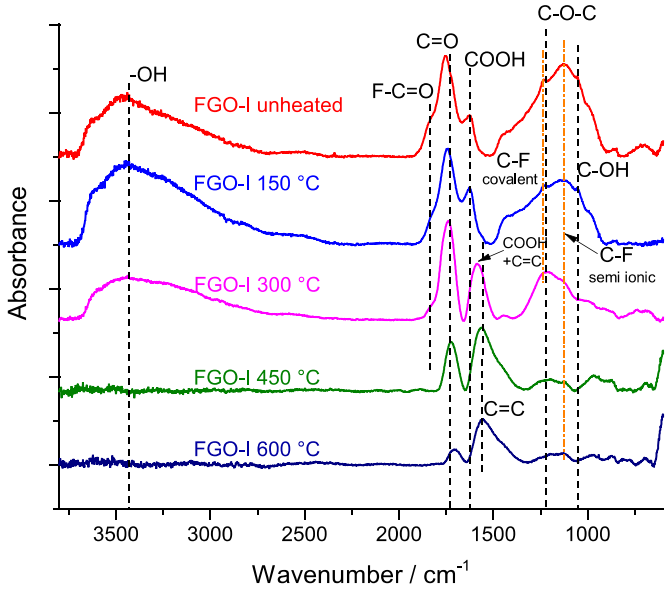

Fig. 5. FTIR-ATR of FGO-I (by XeF_2 for 1300 min) after heating to different temperatures.

for a small peak corresponding to semi-ionic C–F bond. Therefore, both covalent and semi-ionic C–F bonds decomposed, and some of the stronger C–F covalent bond might transform to less stable C–F semi-ionic bond during the heating process.

Little change in oxygen functional groups was found between the unheated samples and those heated to 150 °C. Hydroxyl groups (–OH, 3000–3700 cm^{-1}, C–OH, 1050–1060 cm^{-1}) were significantly reduced between 150 and 300 °C and almost disappeared when heated to 450 °C. A similar trend occurred for the peak of carbolic acid (–COOH, 1620 cm^{-1}). It overlapped with alkane bond (C=C, 1580 cm^{-1}) peak when the sample was heated to 300 °C, giving a peak between 1580 and 1620 cm^{-1}. When the sample was heated to higher temperature (450 and 600 °C), the peak of carbonyl groups (–C=O, 1730 cm^{-1}) and ether groups (C–O–C, 1220 cm^{-1}) decreased significantly, indicating their decomposition at elevated temperature.

T-Jump TOFMS was employed to confirm the release of fluorine during the decomposition process found in DSC-TGA. FGO-I was dispersed in IPA under sonication right after XeF_2 fluorination to avoid any further contact with environmental moisture. The HF^+ fluorine peak appeared in the integrated mass spectrum in Fig. 6(A), confirming the existence of fluorine in the XeF_2 treated sample. Note that H_2O^+, N_2^+ and NO^+ peaks represent unavoidable background signals. C^+, O^+, CO^+ and CO_2^+ arise from the decomposition GO and the oxygen functional groups. Additionally, the time-resolved intensity curve in Fig. 6(B) clearly showed that the fluorine content was released simultaneously with CO_2^+. We may conclude that release of fluorine species occurs simultaneously with decomposition of GO, with an onset temperature of about 265 ± 50 °C, consistent with the decomposition at 245 °C found by the DTG and DSC results. It is interesting that mass loss started below 150 °C in DSC-TGA, while the presence of the fluorine ion in mass spectrometry appeared above 250 °C. It is reasonable to consider that some fluorine loss occurred during the sample preparation for mass spectrometry, especially the most loosely bound species that may escape at reduced temperatures.

Due to the high fraction of oxygen functional groups retained after fluorination, the FGO samples can be dispersed in a variety of solvents under sonication, shown in Figure S4. The dispersing behavior of FGO was similar like that of GO [50], which enhances its potential application by dispersing in different kinds of solvents. FTIR and SEM-EDS analysis of the vacuum-dried dispersions prepared in IPA, THF, propylene carbonate (PC), and cyclohexane were then obtained to determine the change in composition during sonication. All solvents were dried by molecular sieve before using. The results are shown in Fig. S5 and Table S2. It is clear that extra C–H peaks showed up in all dried FGO dispersions as evidenced from 2800 to 3000 cm^{-1} in FTIR curves, which was absent in the FTIR curve of FGO-I, indicating that some solvent might be trapped or bonded in the dried sample. Moreover, the peak of acyl fluoride at 1840 cm^{-1} of FGO-I in Fig. 3 almost disappeared, confirming the decomposition of acyl fluoride during sonication. Therefore, the fluorine species that loosely intercalated or bonded between graphene sheets escaped from the structure during the exfoliation of graphene under sonication. As a result, the fluorine content dropped from more than 10% in FGO-I to only 1–3.5% in these dried dispersions. The F/O ratio also dropped from 0.3 to only about 0.1. The remained fluorine content mostly existed in C-F covalent and semi-ionic bonds, which are thermally more stable.

These results indicate that XeF_2 can be employed as a means for the fluorination of GO to FGO while retaining a majority of oxygen functional groups. However, the fluorine content in the material degraded with time in the presence of even a relatively small quantity of water vapor (15% humidity at 25 °C). Part of the fluorine content formed acyl fluoride and can be easily hydrolyzed with the moisture in atmosphere or can react with solvent during dispersing process for further utilization. Almost 40% of fluorine escaped from the material when heated to 150 °C. Despite the loss of acyl fluoride during heating, some fluorine structures

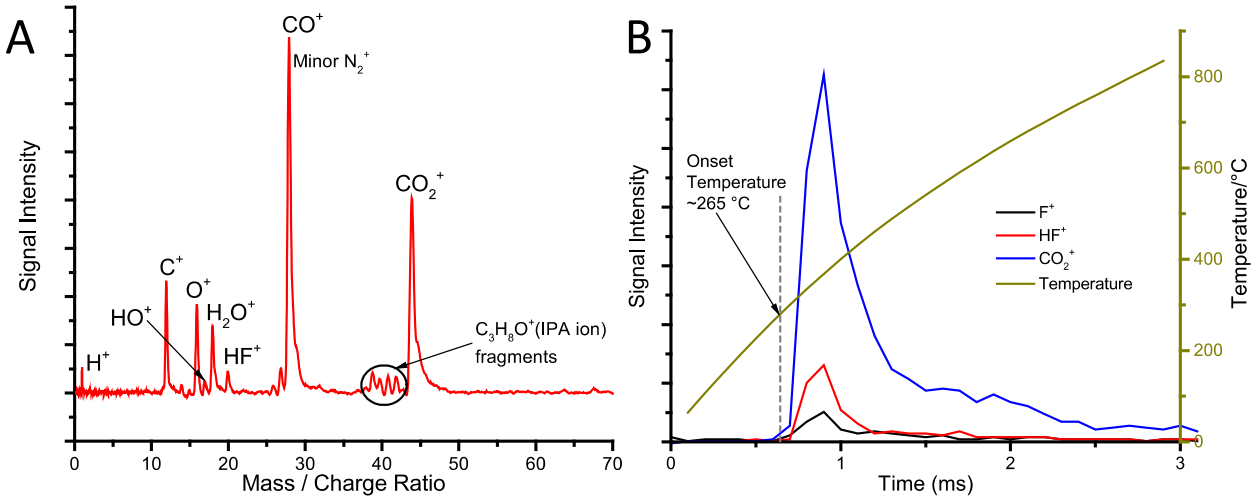

Fig. 6. Integrated (A) and time-resolved (B) mass spectrometry results of FGO-I dispersed in IPA.

Table 2
Energetic samples measured by DSC-TGA with different compositions. GR stands for graphene-rich, and FR stands for fuel-rich.

Sample name and mass ratio	Mass (Total mass = 100 mg)			Remark
	GO/FGO	Al (80% active)	Bi_2O_3	
GO/Al-GR (70/30)	70 mg	30 mg	0	
FGO-I/Al-GR (70/30)	70 mg	30 mg	0	
GO/Al-FR (30/97)	23.5 mg	76.5 mg	0	GO(FGO)/Al ratio same as in GO(FGO)/Al/Bi_2O_3.
FGO-I/Al-FR (30/97)	23.5 mg	76.5 mg	0	
GO/Al/Bi_2O_3 (30/97/473)	5 mg	16.2 mg	78.8 mg	5% GO(FGO) by mass. Equivalence ratio (ER) of Al/Bi_2O_3 = 1.4.
FGO-I/Al/Bi_2O_3 (30/97/473)	5 mg	16.2 mg	78.8 mg	
Al/Bi_2O_3 (97/473)	0	17 mg	83 mg	ER of Al/Bi_2O_3 = 1.4.

such as H-F molecules which are not strongly chemically bonded to graphene plane might exist in the structure. This fluorine content can be easily removed from the structure under heating to low temperature, during the exfoliation of graphene sheets under sonication, or even during storage. Therefore, fluorine showed significantly reduced stability when compared to oxygen in the FGO synthesized by GO with XeF_2.

One of the potential applications of FGO is as a component in nanoenergetic formulations. Al nanoparticles are a common fuel and possesses a naturally formed inert Al_2O_3 shell on its surface, which protects the Al core from further oxidation under ambient conditions. Unfortunately, the shell also acts as a reaction limiting barrier between fuel Al and oxidizer. Fluorine, however, may act to remove or weaken the Al_2O_3 shell and accelerate the reaction with solid state oxide (Al_2O_3 + "F" → AlF_3 + O, where "F" indicates a highly reactive fluorine species, and O indicates produced oxygen composites) [42]. To investigate the role of FGO additives in nanoenergetic materials, DSC-TGA measurements were carried out on samples composed of GO, FGO, Al and Bi_2O_3, as summarized in Table 2. In these experiments, the relative mass of GO or FGO, Al, and Bi_2O_3 were varied to better understand the role of FGO in the overall reactions. The introduction of Bi_2O_3 was motivated by conventional nanothermite composites that utilize a solid-state oxidizer to initiate the exothermic reaction with Al fuel.

A representative DSC curve of GO/Al-GR (Fig. 7(A), GR stands for graphene-rich) shows no significant reaction before melting of Al. The small exotherms between 500 and 620 °C resulted from reaction between the Al core and generated OH species such as H_2O from GO, mainly from the decomposition of hydroxyl groups bonded in GO structure. These species were adsorbed on the amorphous alumina shell and reacted with Al when the core started to diffuse as the temperature was elevated above 500 °C, giving the small exotherms observed. A sharp endotherm of Al melting is seen at 660 °C, followed by the main exothermic reaction between Al and GO, indicating that Al primarily reacted in the liquid phase after it may readily flow out of the shell. When GO was replaced by FGO-I, the DSC indicated that the largest exothermic reaction occurred before the melting of Al. The main reaction peak between 610 and 660 °C indicated that Al_2O_3 shell was weakened by the fluorine species generated from FGO-I decomposition. The expanding Al at elevated temperature was then allowed to diffuse out from the shell before reaching its melting point. The disappearance of the small exotherms between 500 and 620 °C in FGO-I/Al- GR compared to GO/Al-GR was due to the removal of hydroxyl groups during fluorination. Al was not fully reacted before its melting, indicating that the fluorine and oxygen content in FGO-I was not sufficient to weaken or remove all alumina shells prior to Al melting. Some Al melted and then reacted with graphene. The total reaction energy between the two samples was similar (118 J/g for GO/Al-GR and 104 J/g for FGO-I/Al-GR), but the fraction of energy released before and after Al melting varied significantly between the two materials.

As an additive in nanothermite composite, graphene or functionalized graphene is usually no more than 5% mass with Al and metal oxide [34], or no more than 30% mass with Al only [51] to obtain optimized energetic performance. When assembling a composite of only GO/FGO and Al, we analyzed the DSC of samples with 23.5% FGO (GO) by mass, labeled GO/Al – FR and FGO-I/Al – FR (FR stands for fuel-rich), as shown in Fig. S6. The GO/Al – FR showed an exotherm between 520 and 600 °C, as a result of the decomposed OH species penetrating the shell and reacting with the Al, similar to GO/Al – GR. Unlike in the sample with 70% of FGO (FGO-I/Al-GR) described previously, the fluorine content in the composite FGO-I/Al – FR was not enough to react extensively with

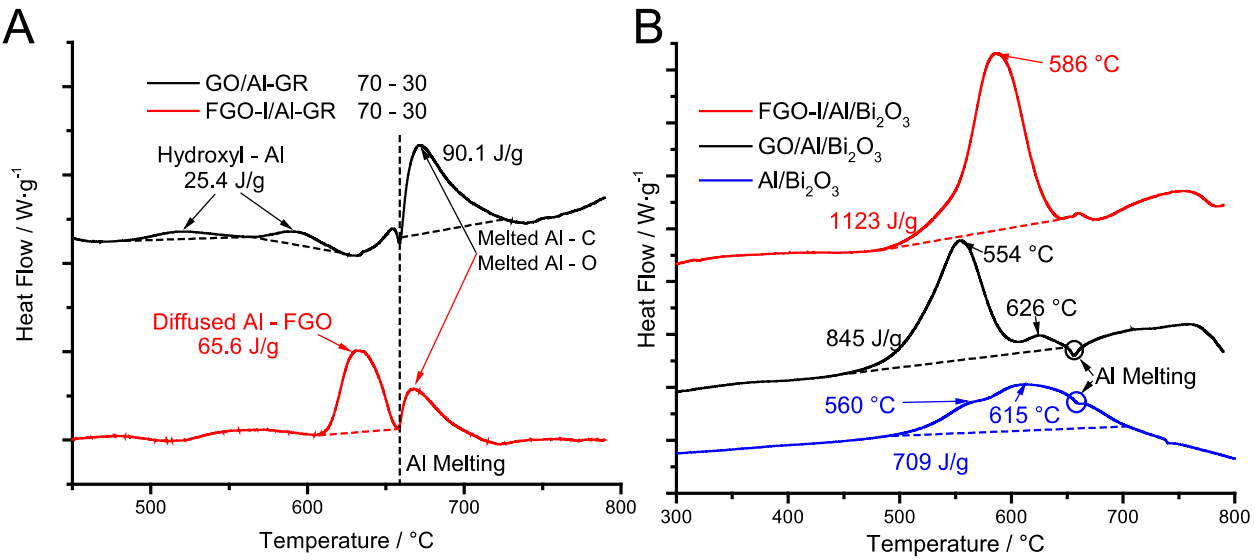

Fig. 7. DSC results of GO/Al-GR and FGO-I/Al – GR (A) and FGO-I/Al/Bi_2O_3, GO/Al/Bi_2O_3 and Al/Bi_2O_3 (B). Upward is exothermic.

diffusing Al after reacting with the alumina shell. Therefore, there was not a dominating exothermic reaction in DSC in Figure S6B like in Fig. 7(A) (FGO/Al-GR) before Al melting. However, a small exotherm was observed around 610 °C, which is close to the large exothermic peak in Fig. 7(A) (FGO/Al-GR). This result indicated that the Al core was able to diffuse out from the shell easier and react with the FGO surrounding it before reaching melting, even the amount of FGO-I was only about 1/3 in mass compared to Al.

Based on calculation shown in supporting information, the 3% fluorine in FGO by mass was not enough to react completely with the Al_2O_3 shell of Al in any of the samples listed in Table 2. We note, however, that the alumina shell does not need to be completely removed to facilitate enhanced reactions. Small pinholes or thinned walls could sufficiently accelerate the diffusion of the Al core out of the shell before its melting. As we discussed above, 3% of fluorine in FGO in FGO-I/Al-FR was sufficient to react Al in the solid state. A similar scenario is present if a secondary oxidizer such as Bi_2O_3 was added to the FGO/Al composite. Partial removal or thinning of the Al_2O_3 shell by fluorine from FGO was sufficient to enable the Al/Bi_2O_3 reaction at a temperature at which Al is in the solid state.

Bi_2O_3 nanoparticles are commonly used in Al-based nanoenergetic composites due to its reaction and pressurization rate [34,35,52]. Introduction of Bi_2O_3 nanoparticles provided a robust solid-state oxidizer with which Al can react after escaping the Al_2O_3 encapsulating shell. Fig. 7(B) shows the reaction heat of Al/Bi_2O_3 nanothermite with GO and FGO-I additives. In Al/Bi_2O_3 loose powder, the reaction initiated at 500 °C due to the start of Al core diffusion out of the shell, peaked at around 615 °C and was completed at about 700 °C after the melting of Al. Neat Al/Bi_2O_3 mixtures are known to be inhomogeneous as a result of phase separation [34,35]. The low-temperature reaction likely occurred between surface contacted Al and Bi_2O_3 nanoparticles, while part of reaction occurred after the melting and free flow of Al [35]. When GO was added to the Al/Bi_2O_3 nanocomposite mixture, GO/Al/Bi_2O_3 showed the lowest onset exothermic temperature around 460 °C, similar to that observed previously when testing GO/Al (70–30). OH species released from GO reacted with diffused Al in the Al_2O_3 shell when the sample was heated to about 480 °C. The local exothermic reactions further accelerated the diffusion and reaction of Al core. The total energy release of GO/Al/Bi_2O_3 was enhanced by approximately 20% compared to neat Al/Bi_2O_3 due to the reduced phase separation as a result of GO addition [34]. The improved Al and Bi_2O_3 intermixing in the presence of GO reduced diffusion length scales for mass transport and the peak reaction temperature for the GO/Al/Bi_2O_3 compared to Al/Bi_2O_3 [34]. After the first reaction, GO/Al/Bi_2O_3 showed a second reaction peaking at 626 °C as Al reacted with Bi_2O_3 particles which were not in direct contact prior to reaction. It is notable that the melting peak of Al was observed in both Al/Bi_2O_3 loose powder and GO/Al/Bi_2O_3, indicating that part of the Al core remained unreacted prior the melting point of Al at 660 °C. With the addition of FGO-I, the melting peak of Al was not observed, and the reaction was nearly completed before the melting temperature of Al. Because fluorine reacted with the alumina shells, solid state Al escaped from the Al_2O_3 shell and reacted with Bi_2O_3 nanoparticles at an onset temperature of 480 °C and peak reaction temperature of 586 °C, both prior to the onset of the Al melting temperature. Due to the absence of OH groups after XeF_2 fluorination, the reaction onset temperature of FGO-I/Al/Bi_2O_3 was greater than that of GO/Al/Bi_2O_3. However, the weakened Al_2O_3 shell provided by fluorine species lowered the onset temperature relative to Al/Bi_2O_3. Moreover, FGO/Al/Bi_2O_3 showed a total energy release of over 1100 J/g, which was 60% higher than Al/Bi_2O_3 loose powder and 33% higher than GO/Al/Bi_2O_3.

4. Conclusion

Fluorination of GO was achieved using low-pressure processing in XeF_2 gas, and the resulting FGO was then incorporated in nanothermite composites to provide both a nanoparticle assembly scaffold and a source of reactive fluorinated species. The XeF_2 process retained the GO oxygen functional groups, enabling the easy dispersion of fluorinated GO in different solvents while also facilitating further chemical functionalization. The fluorine functional groups in the FGO, identified by FTIR, included acyl fluoride groups, carbon-fluorine covalent and semi-ionic bonds. The intercalated fluorine and highly reactive acyl fluoride in the structure were loosely bound and were reactive with atmospheric moisture, mild heating, or mild sonication. When FGO is introduced into a nanothermite composite, the fluorine species supplied by the FGO acted to etch the Al_2O_3 shell of Al nanoparticles at temperatures below the melting temperature of Al. Mass spectrometry measurements indicate that fluorine species were released at ap-

proximately 265 °C, concurrent with the generation of CO_2^- from FGO decomposition. DSC measurements further showed a reduction in reaction temperature with the addition of FGO and that all Al reacted prior to the Al melting temperature in FGO/Al/Bi_2O_3 composites. Further, the all solid-state reaction between Al and Bi_2O_3 in the FGO/Al/Bi_2O_3 composites produced 58% greater energy release than Al/Bi_2O_3 loose powder. The increased energy release is attributed to both the presence of reactive fluorine species and the role of the FGO to act as an assembly template for Al and Bi_2O_3 nanoparticles to increase particle intimacy while reducing phase separation. The chemical functionalization of nanothermite assembly scaffold materials, including fluorinated GO, represents a new mechanism to control energetic material response.

Declaration of Competing Interest

The authors declare that they have no known competing financial interests or personal relationships that could have appeared to influence the work reported in this paper.

The authors declare the following financial interests/personal relationships which may be considered as potential competing interests.

Acknowledgment

This project is sponsored by the Air Force Office of Scientific Research (Grant No. FA9550-16-1-0146).

Supplementary materials

Supplementary material associated with this article can be found, in the online version, at doi:10.1016/j.combustflame.2020.02.005.

References

[1] O. Ruff, O. Bretschneider, Die reaktionsprodukte der verschiedenen kohlenstoffformen mit fluor ii (Kohlenstoff-monofluorid), Zeitschrift für anorganische und allgemeine Chemie 217 (1934) 1–18.
[2] A.M. Panich, Nuclear magnetic resonance study of fluorine–graphite intercalation compounds and graphite fluorides, Synth. Met. 100 (1999) 169–185.
[3] W. Tiedemann, Electrochemical behavior of the fluorographite electrode in nonaqueous media, J. Electrochem. Soc. 121 (1974) 1308–1311.
[4] R.J. Lagow, R.B. Badachhape, J.L. Wood, J.L. Margrave, Some new synthetic approaches to graphite-fluorine chemistry, J. Chem. Soc. Dalton Trans. (1974) 1268–1273, doi:10.1039/DT9740001268.
[5] W. Rüdorff, Graphite intercalation compounds, in: H.J. Emeléus, A.G. Sharpe (Eds.), Advances in Inorganic Chemistry and Radiochemistry, Academic Press, 1959, pp. 223–266.
[6] H.E. Sliney, Graphite fluoride (CFx)n – A New solid lubricant au - Fusaro, robert l, ASLE Trans. 13 (1970) 56–65.
[7] X. Chia, A. Ambrosi, M. Otyepka, R. Zbořil, M. Pumera, Fluorographites (CFx)n exhibit improved heterogeneous electron-transfer rates with increasing level of fluorination: towards the sensing of biomolecules, Chem. Eur. J. 20 (2014) 6665–6671.
[8] C. Delabarre, M. Dubois, J. Giraudet, K. Guérin, A. Hamwi, Electrochemical performance of low temperature fluorinated graphites used as cathode in primary lithium batteries, Carbon NY 44 (2006) 2543–2548.
[9] S. Ebnesajjad, Expanded PTFE Applications Handbook: Technology, Manufacturing and Applications, Elsevier, 2016.
[10] A.L. Logothetis, Chemistry of fluorocarbon elastomers, Prog. Polym. Sci. 14 (1989) 251–296.
[11] C.D. James, G.W. Franklin, Fluorocarbon Vinyl Ether Polymers, United Stated, 1967.
[12] R. Taylor, J.H. Holloway, E.G. Hope, A.G. Avent, G.J. Langley, T.J. Dennis, J.P. Hare, H.W. Kroto, D.R.M. Walton, Nucleophilic substitution of fluorinated C60, J. Chem. Soc. Chem. Commun. (1992) 665–667, doi:10.1039/C39920000665.
[13] A. Hamwi, H. Alvergnat, S. Bonnamy, F. Béguin, Fluorination of carbon nanotubes, Carbon N Y 35 (1997) 723–728.
[14] E.T. Mickelson, C.B. Huffman, A.G. Rinzler, R.E. Smalley, R.H. Hauge, J.L. Margrave, Fluorination of single-wall carbon nanotubes, Chem. Phys. Lett. 296 (1998) 188–194.
[15] J.T. Robinson, J.S. Burgess, C.E. Junkermeier, S.C. Badescu, T.L. Reinecke, F.K. Perkins, M.K. Zalalutdniov, J.W. Baldwin, J.C. Culbertson, P.E. Sheehan, E.S. Snow, Properties of fluorinated graphene films, Nano Lett. 10 (2010) 3001–3005.
[16] X. Yang, X. Jia, X. Ji, Acid induced fluorinated graphene oxide, RSC Adv. 5 (2015) 9337–9340.
[17] A.K. Geim, K.S. Novoselov, The rise of graphene, Nat. Mater. 6 (2007) 183–191.
[18] K.P. Loh, Q. Bao, P.K. Ang, J. Yang, The chemistry of graphene, J. Mater. Chem. 20 (2010) 2277–2289.
[19] H. An, Y. Li, P. Long, Y. Gao, C. Qin, C. Cao, Y. Feng, W. Feng, Hydrothermal preparation of fluorinated graphene hydrogel for high-performance supercapacitors, J. Power Sources 312 (2016) 146–155.
[20] S. Huang, Y. Li, Y. Feng, H. An, P. Long, C. Qin, W. Feng, Nitrogen and fluorine co-doped graphene as a high-performance anode material for lithium-ion batteries, J. Mater. Chem. A 3 (2015) 23095–23105.
[21] N. Liaros, A.B. Bourlinos, R. Zboril, S. Couris, Fluoro-graphene: nonlinear optical properties, Opt. Express 21 (2013) 21027–21038.
[22] F. Withers, M. Dubois, A.K. Savchenko, Electron properties of fluorinated single-layer graphene transistors, Phys. Rev. B 82 (2010) 073403.
[23] W. Feng, P. Long, Y. Feng, Y. Li, Two-Dimensional fluorinated graphene: synthesis, structures, properties and applications, Adv. Sci. 3 (2016) 1500413.
[24] X. Wang, Y. Dai, J. Gao, J. Huang, B. Li, C. Fan, J. Yang, X. Liu, High-Yield production of highly fluorinated graphene by direct heating fluorination of graphene-oxide, ACS Appl. Mater. Interfaces 5 (2013) 8294–8299.
[25] R. Stine, W.-K. Lee, K.E. Whitener, J.T. Robinson, P.E. Sheehan, Chemical stability of graphene fluoride produced by exposure to xef2, Nano Lett. 13 (2013) 4311–4316.
[26] Y.-Y. Yu, B.H. Kang, Y.D. Lee, S.B. Lee, B.-K. Ju, Effect of fluorine plasma treatment with chemically reduced graphene oxide thin films as hole transport layer in organic solar cells, Appl. Surf. Sci. 287 (2013) 91–96.
[27] S.B. Bon, L. Valentini, R. Verdejo, J.L. Garcia Fierro, L. Peponi, M.A. Lopez–Manchado, J.M. Kenny, Plasma fluorination of chemically derived graphene sheets and subsequent modification with butylamine, Chem. Mater. 21 (2009) 3433–3438.
[28] K. Tahara, T. Iwasaki, A. Matsutani, M. Hatano, Effect of radical fluorination on mono- and bi-layer graphene in ar/f2 plasma, Appl. Phys. Lett. 101 (2012) 163105.
[29] Z. Wang, J. Wang, Z. Li, P. Gong, X. Liu, L. Zhang, J. Ren, H. Wang, S. Yang, Synthesis of fluorinated graphene with tunable degree of fluorination, Carbon NY 50 (2012) 5403–5410.
[30] K. Samanta, S. Some, Y. Kim, Y. Yoon, M. Min, S.M. Lee, Y. Park, H. Lee, Highly hydrophilic and insulating fluorinated reduced graphene oxide, Chem. Commun. 49 (2013) 8991–8993.
[31] P. Gong, Z. Wang, Z. Li, Y. Mi, J. Sun, L. Niu, H. Wang, J. Wang, S. Yang, Photochemical synthesis of fluorinated graphene via a simultaneous fluorination and reduction route, RSC Adv. 3 (2013) 6327–6330.
[32] M. Dubois, K. Guérin, Y. Ahmad, N. Batisse, M. Mar, L. Frezet, W. Hourani, J.-L. Bubendorff, J. Parmentier, S. Hajjar-Garreau, L. Simon, Thermal exfoliation of fluorinated graphite, Carbon NY 77 (2014) 688–704.
[33] C. Sun, Y. Feng, Y. Li, C. Qin, Q. Zhang, W. Feng, Solvothermally exfoliated fluorographene for high-performance lithium primary batteries, Nanoscale 6 (2014) 2634–2641.
[34] R. Thiruvengadathan, S.W. Chung, S. Basuray, B. Balasubramanian, C.S. Staley, K. Gangopadhyay, S. Gangopadhyay, A versatile self-assembly approach toward high performance nanoenergetic composite using functionalized graphene, Langmuir 30 (2014) 6556–6564.
[35] A. Wang, S. Bok, R. Thiruvengadathan, K. Gangopadhyay, J.A. McFarland, M.R. Maschmann, S. Gangopadhyay, Reactive nanoenergetic graphene aerogel synthesized by one-step chemical reduction, Combust. Flame 196 (2018) 400–406.
[36] Y. Chen, G.C. Egan, J. Wan, S. Zhu, R.J. Jacob, W. Zhou, J. Dai, Y. Wang, V.A. Danner, Y. Yao, K. Fu, Y. Wang, W. Bao, T. Li, M.R. Zachariah, L. Hu, Ultra-fast self-assembly and stabilization of reactive nanoparticles in reduced graphene oxide films, Nat. Commun. 7 (2016) 12332.
[37] J. Shen, Z. Qiao, J. Wang, G. Yang, J. Chen, Z. Li, X. Liao, H. Wang, M.R. Zachariah, Reaction mechanism of al-cuo nanothermites with addition of multilayer graphene, Thermochim. Acta 666 (2018) 60–65.
[38] S. Apperson, R.V. Shende, S. Subramanian, D. Tappmeyer, S. Gangopadhyay, Z. Chen, K. Gangopadhyay, P. Redner, S. Nicholich, D. Kapoor, Generation of fast propagating combustion and shock waves with copper oxide/aluminum nanothermite composites, Appl. Phys. Lett. 91 (2007) 243109.
[39] K.T. Sullivan, N.W. Piekiel, C. Wu, S. Chowdhury, S.T. Kelly, T.C. Hufnagel, K. Fezzaa, M.R. Zachariah, Reactive sintering: an important component in the combustion of nanocomposite thermites, Combust. Flame 159 (2012) 2–15.
[40] G.C. Egan, K.T. Sullivan, T. LaGrange, B.W. Reed, M.R. Zachariah, In situ imaging of ultra-fast loss of nanostructure in nanoparticle aggregates, J. Appl. Phys. 115 (2014) 6.
[41] V.I. Levitas, Burn time of aluminum nanoparticles: strong effect of the heating rate and melt-dispersion mechanism, Combust. Flame 156 (2009) 543–546.
[42] M.L. Pantoya, S.W. Dean, The influence of alumina passivation on nano-Al/Teflon reactions, Thermochim. Acta 493 (2009) 109–110.
[43] B. Chen, H. Zheng, M. Riehn, S. Bok, K. Gangopadhyay, M.R. Maschmann, S. Gangopadhyay, In situ characterization of photothermal nanoenergetic combustion on a plasmonic microchip, ACS Appl. Mater. Interfaces 10 (2018) 427–436.
[44] G.C. Egan, T. LaGrange, M.R. Zachariah, Time-Resolved nanosecond imaging of nanoscale condensed phase reaction, J. Phys. Chem. C 119 (2015) 2792–2797.
[45] A.P. Kharitonov, Practical applications of the direct fluorination of polymers, J. Fluor. Chem. 103 (2000) 123–127.

[46] W. Zhang, P. Bonnet, M. Dubois, C.P. Ewels, K. Guérin, E. Petit, J.-Y. Mevellec, L. Vidal, D.A. Ivanov, A. Hamwi, Comparative study of swcnt fluorination by atomic and molecular fluorine, Chem. Mater. 24 (2012) 1744–1751.
[47] M. Adamska, U. Narkiewicz, Fluorination of carbon nanotubes – A review, J. Fluor. Chem. 200 (2017) 179–189.
[48] S. Park, J. An, J.R. Potts, A. Velamakanni, S. Murali, R.S. Ruoff, Hydrazine-reduction of graphite- and graphene oxide, Carbon NY 49 (2011) 3019–3023.
[49] M.P. Araújo, O.S.G.P. Soares, A.J.S. Fernandes, M.F.R. Pereira, C. Freire, Tuning the surface chemistry of graphene flakes: new strategies for selective oxidation, RSC Adv. 7 (2017) 14290–14301.
[50] J.I. Paredes, S. Villar-Rodil, A. Martinez-Alonso, J.M.D. Tascon, Graphene oxide dispersions in organic solvents, Langmuir 24 (2008) 10560–10564.
[51] Y. Jiang, S. Deng, S. Hong, J. Zhao, S. Huang, C.-C. Wu, J.L. Gottfried, K.-i. Nomura, Y. Li, S. Tiwari, R.K. Kalia, P. Vashishta, A. Nakano, X. Zheng, Energetic performance of optically activated aluminum/graphene oxide composites, ACS Nano 12 (2018) 11366–11375.
[52] R. Thiruvengadathan, C. Staley, J.M. Geeson, S. Chung, K.E. Raymond, K. Gangopadhyay, S. Gangopadhyay, Enhanced combustion characteristics of bismuth trioxide-aluminum nanocomposites prepared through graphene oxide directed self-assembly, Propell. Explos. Pyrotech. 40 (2015) 729–734.